journal

J. Am. Ceram. Soc., 1–6 (2011)
DOI: 10.1111/j.1551-2916.2011.04993.x

Ice-Templating of Alumina Suspensions: Effect of Supercooling and Crystal Growth During the Initial Freezing Regime

Audrey Lasalle,[‡,†] Christian Guizard,[‡] Jérôme Leloup,[‡] Sylvain Deville,[‡] Eric Maire,[§] Agnès Bogner,[§] Catherine Gauthier,[§] Jérôme Adrien,[§] and Loïc Courtois[§]

[‡]Laboratoire de Synthèse et Fonctionnalisation des Céramiques, UMR 3080 CNRS/Saint-Gobain, 84306 Cavaillon, France

[§]INSA-Lyon, MATEIS CNRS UMR5510, Université de Lyon, F-69621 Villeurbanne, France

We investigate the ice-templating behavior of alumina suspensions by *in situ* X-ray radiography and tomography. We focus herein on the formation and structure of the transitional zone, occurring during the initial instants of freezing. For many applications, this zone is undesirable as the resulting porosity is heterogeneous in size, morphology, and orientation. We investigate the influence of the composition of alumina suspensions on the formation of the transitional zone. Alumina particles are dispersed by three different dispersants, in various quantities, or by chlorhydric acid. We show that the dimensions and the morphology of the transitional zone are determined by the growth of large dendritic ice-crystals growing in a supercooled state much faster than the cellular freezing front. When the freezing temperature decreases, the degree of supercooling increases. This results in an initial faster freezing front velocity and increase in the dimensions of the transitional zone. It is therefore possible to adjust the dimensions of the transitional zone by changing the composition of alumina suspensions. The counter-ion Na^+ has the most dramatic effect on the freezing temperature of suspensions, yielding a predominance of cellular ice crystals instead of the usual lamellar crystals.

I. Introduction

Ice-templating is a shaping process used to obtain porous materials by freezing a suspension of particles and subsequently removing the ice-crystals by freeze-drying. The potential interest for ceramic materials was discovered by Fukasawa in 2001.[1] This process consists of pouring a ceramic suspension into a mold, usually frozen by the bottom. Ice crystals grow unidirectionally, through the suspension, rejecting and concentrating particles in the intercrystals space. Ice crystals are then removed by sublimation. A porous green body is thus obtained where the pores are a direct replica of the ice crystals. The green body can then be consolidated by sintering,[2] if needed. Different pore sizes (from 1 to 100 μm), porosity (from 10% to 90%), and pore morphologies can be obtained. Such materials are currently considered for biomedical applications,[3] active substance delivery,[4] acoustic insulation,[5] SOFC,[6,7] or piezoelectric applications.[8]

The present study rationalizes our early work about the transient regime.[9] We have shown that, during ice-templating, freezing occurs in two stages: an initial transient regime followed by a steady state.[10] During the initial instants of freezing, the freezing front advances quickly in the direction Z imposed by the thermal gradient. The microstructure obtained is characterized by two populations of ice crystals: R-crystals (R for randomly oriented) and Z-crystals (for lamellar ice crystals, oriented along the Z direction). We considered that the ice crystals are oriented when they grow according to the thermal gradient, a direction referred to as direction Z. Due to their different orientation and morphology, these two populations of crystals do not concentrate ceramic particles with the same efficiency. We have shown that the sudden extinction of the R-crystals marks the end of the transitional zone, leaving only lamellar crystals growing into the suspension [figure 5 of the Ref. (9)]. This corresponds to the beginning of the steady state of the freezing. This study has defined the morphological characteristics of the transition zone, but the understanding of its formation mechanism has yet to be explained and the eventual role of the composition of the suspension assessed.

For many applications, a continuous porosity is desired. The presence of a graded structure, corresponding to this transitional zone, can be problematic. For instance, in the SOFC design currently investigated by NASA,[7] the transitional zone limits the efficiency of the infiltration of the porous electrodes obtained by ice-templating.

Several parameters were identified to have an influence over this transient regime, such as the particle size,[11] the shape of the cooling ramp (linear, constant, parabolic),[12] or the application of an electric field during freezing.[13] In the present article, we show that the characteristics of this transient regime are controlled by the initial supercooling conditions. We assess the influence of the composition of alumina suspensions, stabilized with various dispersants. We use X-ray radiography and tomography to respectively observe the freezing front behavior and characterize the resulting frozen microstructure. Although the 1.4 μm resolution does not permit to resolve individual particles, it is high enough to provide an accurate observation of ice crystals and concentrated particles' regions.

II. Experimental Procedure

(1) Suspensions Preparation

Alumina powder (Ceralox SPA 0.5; Sasol, Tucson, AZ), D_{50} = 0.3 μm, with a specific surface area of 8 m^2/g, is dispersed in distilled water with an organic dispersant or with chlorhydric acid. The alumina content is always 32 vol%, unless specified. Thirty-two volume percent is an arbitrary chosen value, but including in the range of alumina contents traditionally used for slip-casted and ice-templated materials. We have prepared some suspensions with a higher alumina content of 50 vol% too to observe the effect of the solid content on freezing. This value is under the critical alumina content, 56.6 vol%, above which the particles are no longer rejected by ice crystals but trapped into ice.[14] Three sorts of suspensions are prepared. Some contain an ammonium

H.-E. Kim—contributing editor

Manuscript No. 29789. Received May 27, 2011; approved November 06, 2011.
[†]Author to whom correspondence should be addressed. e-mail: lasalla.andrey@gmail.com

polymethacrylate as dispersant (Darvan CN; Vanderbilt, Norwalk, CT), others contain a sodium polymethacrylate (Darvan 7 Ns; Vanderbilt), and the third type of suspension is dispersed by an ammonium polyacrylate (Darvan 821A; Vanderbilt). These organic dispersants are respectively referred in text as D[NH_4^+], D[Na^+], and d[NH_4^+]. They are introduced with a quantity varying from 0.2 to 2 wt%. Suspensions prepared with chlorhydric acid (HCl) contain 3.1×10^{-2} or 6×10^{-2} mol/L of HCl. Dispersant (or acid) is stirred with distilled water for 30 min and then the alumina powder is added. Alumina suspensions are ball-milled for 40 h, de-aired before being ice-templated. The dispersant quantity is expressed in weight percent related to the mass of dried powder. The various suspensions investigated are summarized in Table I.

(2) Freezing SetUp

Suspensions are introduced into a polypropylene mold of 3 mm in diameter, with a syringe. A particular attention is paid to avoid air bubbles introduction in suspension. The mold is placed on the top of a copper finger cooled from the bottom by a liquid nitrogen circulation. The cooling rate is controlled by the liquid nitrogen flow and the temperature profile is registered during experiment, attributable to a thermocouple located near the copper finger surface. The setup of freezing was previously described.[9] Our measurements have shown that alumina suspensions can be frozen with this setup at a cooling rate ranging from 3 to 5.3°C/min.

(3) Freezing-Temperature Measurement

Two techniques were used for the freezing-temperature measurement. Cold-Differential Scanning Calorimetry (DSC Q100; TA Instruments) was carried out on a constant 15 μL volume, introduced into a capsule. The capsule is cooled at 2 or 5°C/min. The freezing temperature is defined as the beginning of the endothermic peak, determined by the fitting tangent method. We also use a thermocouple located at the surface of the copper finger during the freezing experiment. In this case, the freezing temperature corresponds to the instant where the first ice crystals are observable on the radiographs.

(4) X-Ray Radiography and Tomography

X-ray radiography and tomography experiments were performed at ESRF (Grenoble, France) on the beamline ID-19. A monochromatic high coherent X-ray beam with an energy of 20.5 keV passes through the sample. A CDD camera with 2048 × 2048 sensitive elements is placed at 20 mm behind the sample. The advancement of the freezing front is followed by radiography with a spatial resolution of 2.8 μm. A sequence of pictures is acquired without moving the sample to follow the advancement of the freezing front, so that we can accurately measure the freezing front velocity. In radiography, the gray level is proportional to the transmission of X-rays, i.e. high values of gray levels correspond to a zone with low absorption of X-rays, that is, ice in our case. Low gray levels correspond to the particle-rich phase.

The interest and limitations of the *in situ* X-ray tomography in the field of materials have been demonstrated by Buffière & co. based on the observations of the mechanical behavior of several materials.[15] Tomography consists of acquiring radiographies at different viewing angles during the rotation of a sample over 180°. To ensure a good reconstruction, the microstructure must not evolve during acquisition. If we would perform a tomography acquisition during the freezing, as the scan takes about 10 min, the freezing front would move and the microstructure would evolve during the scan, leading to a poor reconstruction. We therefore observe the microstructure when the sample is completely frozen. The frozen sample is maintained at a constant temperature during the scan. The spatial resolution is 1.4 μm. After a computer treatment, a 3-D map of the absorption coefficient is obtained. Contrarily to radiography, the gray level is proportional to the absorption of X-rays. High gray levels correspond to the phase with the higher atomic number, the particle-rich phase in our case.

(5) Image Analysis

The dimensions (height) of transitional zone are measured from the tomography reconstruction. A sequence of 1600 reconstructed slices of 2048 × 2048 voxels is obtained. Such large files are difficult to handle. The reconstructed images are first scaled to a resolution of 4.7 μm in the X and Y directions perpendicular to the freezing direction. The resolution is preserved in the Z direction to achieve a better accuracy in the measurements of the height of the transitional zone. We then restrict our measurement to a square of 400 × 400 voxels in the X and Y directions. Then, each picture in gray levels is transformed into a binary picture using a segmentation criterion, provided as a plug-in in the software Fiji.[16] A scan of 1600 binarized pictures is obtained. By image analysis, we calculate the fraction of ice and the fraction of the particle-rich phase. By reporting the variation of the particle-rich phase fraction as a function of position Z, we can determine the height of the transitional zone. It is characterized by a rapid decrease in the particle-rich phase fraction, followed by an increase [figure 5 of Ref. (9)]. This sudden variation originates from the extinction of R-crystals, which concentrate particles in the Z direction, while Z-crystals concentrate them mostly in the XY plane, perpendicular to the temperature gradient.

Table I. Composition of the Ice-Templated Alumina Suspensions

Alumina content (vol%)	Nature of additive	Quantity of additive
32	D[NH_4^+]	0.2–0.4–0.7–1–2 wt%
50	D[NH_4^+]	0.2–2 wt%
32	D[Na^+]	0.2–2 wt%
32	d[NH_4^+]	0.2–1 wt%
32	HCI	3.1–6 × 10^{-2} mol/L

III. Results and Discussion

(1) Influence of Ion on the Freezing Temperature

The freezing temperatures lie in the range from −10°C to −20°C, for a cooling rate included between 2 and 5.3°C/min regardless of the composition and the experimental technique (Fig. 1). We can distinguish two ranges of freezing temperature, in the limit of the tested dispersant concentrations, 0.2–2 wt% related to the alumina weight content. First, the −10°C to −15°C range, for example, with the introduction of d[NH_4^+] or HCl with 32 vol% of alumina particles and certain values concerning D[NH_4^+], with 32 or 50 vol% of alumina particles. The second range corresponds to the −15°C to −20°C range. We measured the freezing temperature for suspensions containing dispersant between 0.2 and 2 wt%, where the dispersion state of suspensions could be impacted. The dispersion state was assessed by viscosity and zeta potential measurements, not presented herein. No strong agglomeration was observed since the zeta potential was found in the −45 to −75 mV range, sufficiently high to ensure a stable state and high repulsions between particles. We did not represent the freezing temperature as a function of the dispersant concentration as no clear trend could be identified so far. It appears that the counter-ion Na^+ used in

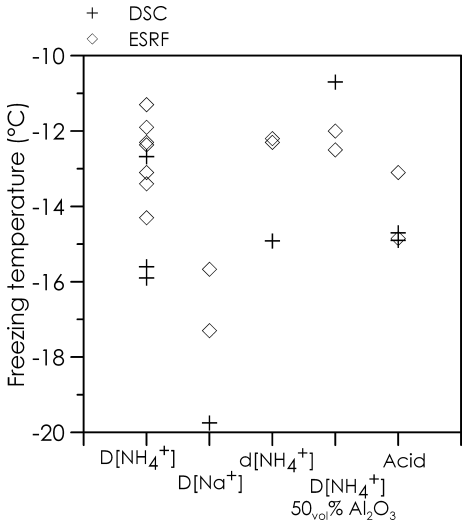

Fig. 1. Freezing temperature of alumina suspensions, measured by cold-DSC (cross points) and by a thermocouple during ERSF experiments (rhomb points). The freezing temperature is measured for different compositions, the dispersant used is reported on the abscissa and all alumina suspensions contain 32 vol% of particles unless specified otherwise.

dispersant is mainly responsible for the decrease in the freezing temperature. Lower freezing temperatures are systematically obtained with this ion. We think the nature of ions is the main parameter controlling the freezing temperature and not the agglomeration state because between 0.2 and 2 wt% of $D[Na^+]$, the freezing temperature is lower than suspensions containing $D[NH_4^+]$ between 0.2 and 2 wt%. For both these dispersants, the agglomeration state of alumina suspensions is similar for similar quantity of dispersant (evaluated by zeta potential and viscosity measurements). So as for similar state of dispersion/agglomeration, the freezing temperature is different; it means that the nature of the ion is the dominant parameter.

To decouple the influence of the dispersant and the influence of the particles, we measured, by cold-DSC only, the freezing temperature of aqueous solutions containing the same quantity of dispersant (or chlorhydric acid) than in the alumina suspensions (Fig. 2). Distilled water freezes between −20°C and −25°C, far from the equilibrium temperature of 0°C, and the addition of dispersant or acid increases the

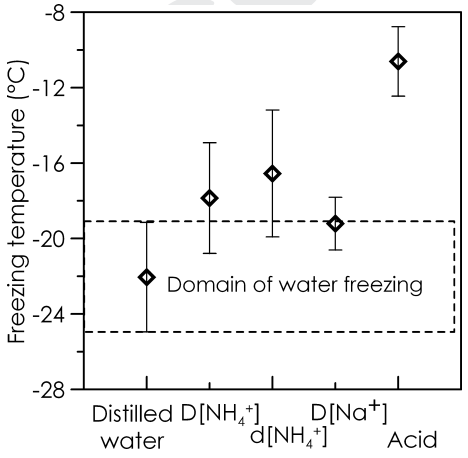

Fig. 2. Freezing temperature obtained by cold-DSC, of aqueous solutions (without alumina particles) containing the same dispersant or acid in similar quantity that alumina suspensions contain. The range within which the distilled water freezes is indicated by a dashed rectangle. The cooling rate is 2°C/min.

freezing temperature. The freezing temperature measured for distilled water can be explained by the specific freezing conditions in the cold-DSC experiments. A very small amount of ultrapure water is put in a clean capsule, so that little nucleation sites are available. It is well established that water can be highly supercooled before the liquid/solid transition occurs. Surfactants (dispersants) and particles incorporated in water act as nucleation sites.[11] The freezing temperature of water, measured in such conditions, cannot be compared with the freezing temperature of the suspensions measured at ESRF. However, we can observe that:

1 the dispersant increases the freezing temperature related to the freezing point of the water,
2 in presence of particles, suspensions containing $D[NH_4^+]$ and $d[NH_4^+]$, freeze at higher temperatures. Hence, particles probably act as heterogeneous nucleation sites,
3 the presence of particles has little impact over the range of freezing temperature of suspensions dispersed with $D[Na^+]$. It means that the effect of ion Na^+ has a stronger impact on the freezing temperature than the addition of particles,
4 with particles, suspensions dispersed with HCl freeze at lower temperatures. No explanations for these results can be proposed at this point.

(2) Relations Between Initial Dendritic Ice Crystals and the End of the Transitional Zone

Careful observation of the radiographies allows us to rationalize the previous observations.[9] When freezing begins, large ice crystals, with a very dendritic morphology, pointed out by white arrows on the right part of Figs. 3(a) and (b), grow very quickly into the suspension. Their growth velocity is five to fifteen times greater than that of the freezing front appearing later. When they stop growing, they partially melt back, the melting starting from the top of the crystals.

Reconstruction of the tomography data shows that the microstructure and magnitude of the transitional zone depend on the composition of the suspension. All investigated formulations are not presented, we focus on the particular effect of $D[Na^+]$ which induces a strong decrease of the freezing temperature. We compare its influence with that of $D[NH_4^+]$ to highlight the effect of the counter-ion Na^+. For the suspension containing 2 wt% $D[NH_4^+]$, we clearly observe the end of the transitional zone, characterized by the apparition of a continuous lamellar morphology [Fig. 4(b)]. A perpendicular cross-section shows a typical microstructure of R-crystals and Z-crystals [Fig. 5(a)]. This microstructure is less well-defined for the suspension with 0.2% $D[NH_4^+]$, but the location of the end of the transitional zone can still be identified. Suspensions containing 0.2 or 2 wt% $D[Na^+]$ [Figs. 4(c) and (d)] have a transitional zone size larger than that of suspensions containing $D[NH_4^+]$ [Figs. 4(a) and (b)]. A perpendicular cross-section shows that the transitional zone comprises only cellular ice crystals. No lamellar ice crystals are observed [Fig. 5(b)].

To understand the role of the large dendritic ice crystals, their dimensions, assessed on the radiography, can be compared with the frozen microstructure of the corresponding zone [Figs. 3(a) and (b)]. Examples of such observations are shown for suspensions containing $D[NH_4^+]$, where the large dendritic crystals are the most visible. We observe that the location where these large ice crystals stop coincides with the location of the end of the transitional zone. When the transitional zone extends beyond the observation window, in the case of suspensions containing $D[Na^+]$, the top of the large dendritic crystals is not observable on the radiographies. It is therefore reasonable to assume that the growth and dimensions of these crystals correspond to the formation and extent of the transitional zone, and that these large crystals

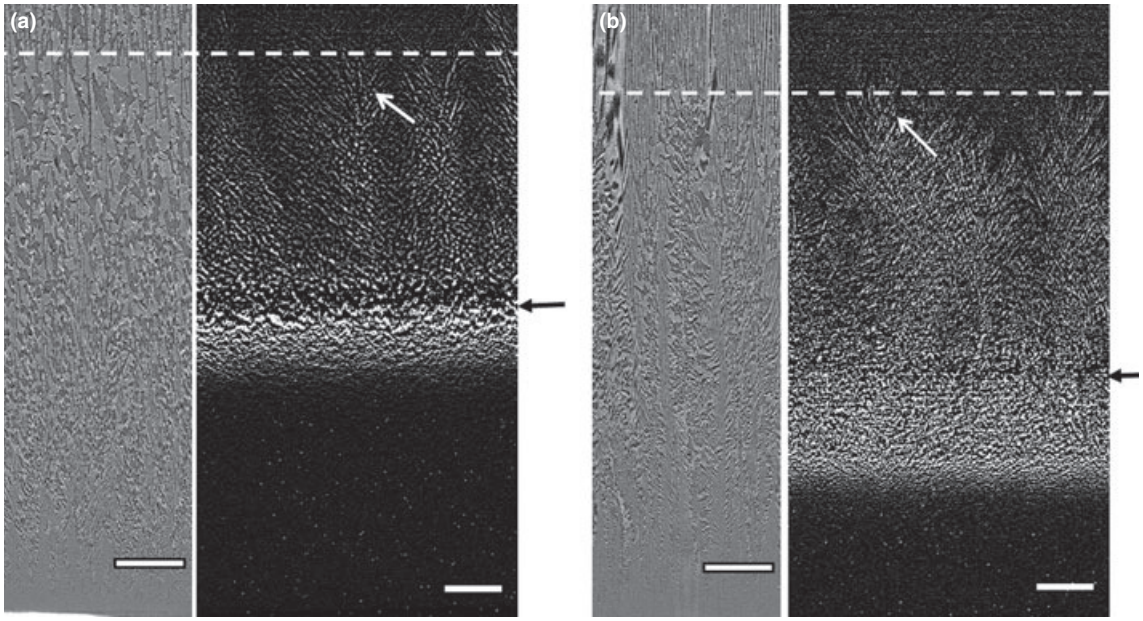

Fig. 3. Binary radiography obtained by subtraction of three consecutive radiographies (right hand side of each image) versus the corresponding reconstructed tomography (left hand side). The dashed line indicates the location where the large dendritic ice crystals (white arrow) stop growing. The black arrows indicate the location of the freezing front. By extending the dashed line on the reconstructed tomography, we observe the large ice crystals stop around the end of the transitional zone. The ice-templated suspensions contain 0.4 wt% D[NH_4^+] (a) and 2 wt% D[NH_4^+] with 32 vol% Al_2O_3 (b). Scale bars = 200μm.

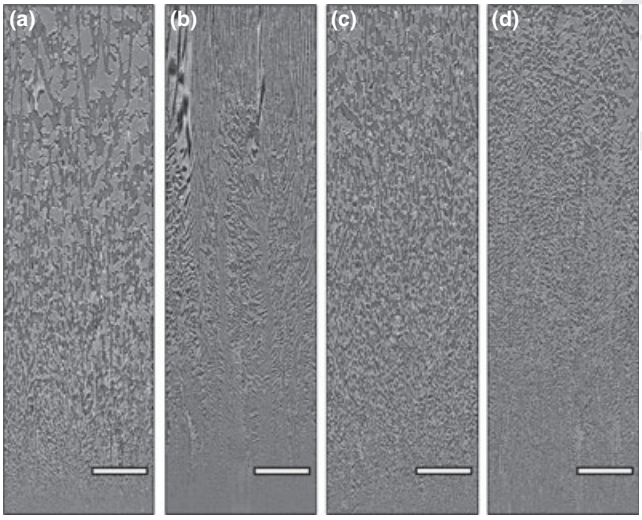

Fig. 4. Cross-sections of reconstructed tomography, parallel to the freezing direction, showing the frozen microstructure of the transitional zone for the alumina suspensions containing 0.2 wt% D[NH_4^+] (a), 2 wt% D[NH_4^+] (b), 0.2 wt% D[Na^+] (c), 2 wt% D[Na^+] (d). The end of the transitional zone can only be observed for the first two suspensions. Scale bars = 200 μm

correspond to the previously identified R-crystals. The large dendritic ice crystals should be the first formed nuclei reaching their critical size. These nuclei are formed in a highly supercooled suspension. The location where their growth comes to a halt should thus correspond to the location where the suspension is at its equilibrium temperature. Similar conclusions were recently drawn by Spannuth *et al.*,[17] using a very different approach. They observed that the transitional zone (referred as stage I in their paper) ends when the sample is warmed to the melting temperature. We can also assume that the top of the large dendritic ice crystals melt back because of the important latent heat released during their growth, locally increasing the temperature. The extinction of the R-crystals marks the end of the transitional zone.[9] Then, we enter in the steady state of the freezing regime. Finally, the dendritic aspect of the R-crystals can be explained by their very high-growth velocity, cellular and dendritic morphology being favored by high-interface velocity.

(3) Freezing Temperature/Supercooling Effect on the Height of the Transitional Zone

We observe a different freezing behavior between suspensions containing D[NH_4^+], d[NH_4^+], or HCl and the suspensions containing D[Na^+]. The presence of Na^+ as a counter-ion in the dispersant has a strong impact on the freezing temperature, decreasing it to about −20°C (Fig. 1). The sodium polymethacrylate is supposed to have an antifreeze activity as the ammonium polyacrylate.[18] This activity could be reinforced by the structuring nature of the sodium cation and its capacity to rearrange molecular water[19] and might thus explain the decrease in the freezing temperature. By decreasing the freezing temperature, the supercooling effect increases. As the first ice crystals appearing do so in a supercooled suspension, they grow very fast to quickly reach their equilibrium position, where the freezing temperature and the temperature in the suspension are equal. The greater the degree of supercooling, the greater the freezing front velocity. We know that the freezing front velocity determines the ice crystal morphology, which is lamellar at intermediate velocity and cellular when the velocity increases. If we report the evolution of the time it takes for the freezing front to propagate through the observation window on the radiography (transit time) as a function of the freezing temperature for every ice-templated suspensions, we can observe that the greater the degree of supercooling (the lower the freezing temperature), the greater the freezing front velocity (low transit time) (Fig. 6). The cellular microstructure [Fig. 5(b)] in the case of D[Na^+] might thus be explained by an increase in the freezing front velocity, due to an important supercooling effect.

We can adjust, to some extent, the dimensions of the transitional zone with the initial degree of supercooling (Fig. 7), which increases when the freezing temperature of alumina suspensions decreases. As the Fig. 1 has showed that there are two ranges of freezing temperature depending to the composition of the suspension, we can use this last to adjust

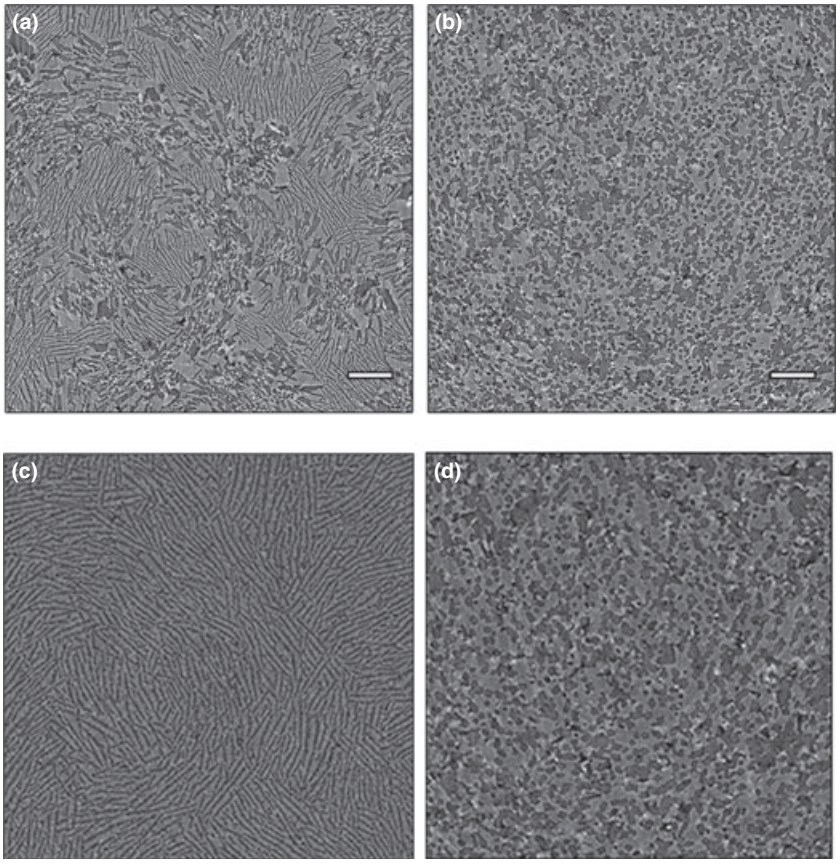

Fig. 5. Cross-sections of reconstructed tomography, perpendicular to the freezing direction, showing the frozen microstructure of the suspension 2 wt% D[NH_4^+] (a, c) and 0.2 wt% D[Na^+] (b, d) in the transitional zone. The first microstructure is a mix between R and Z-crystals (a) which disappear 700 μm higher (c) only Z-crystals remain. Whereas with D[Na^+] no Z-crystals are observed, only cellular R-crystals with a cellular morphology appear (a) even 700 μm higher (d). Hence, the transitional zone is smaller with D[NH_4^+]. Cross-sections were realized at the same height in the transitional zone for a, b. They were taken 700 μm higher for c, d. Scale bar = 200 μm.

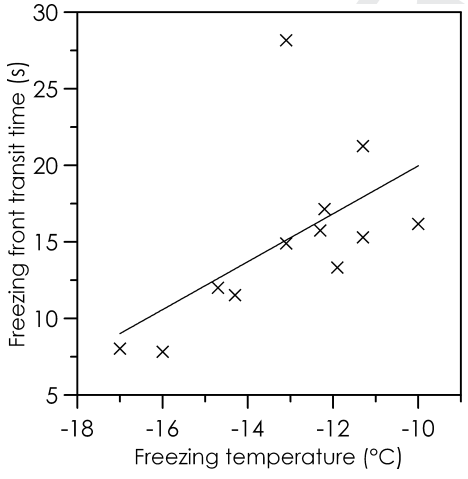

Fig. 6. Freezing front transit time for different suspensions as a function of the freezing temperature measured with a thermocouple. The lower values correspond to suspensions prepared with D[Na^+]. The greater the supercooling, the higher the freezing front velocity, which is inversely proportional to the freezing front transit time.

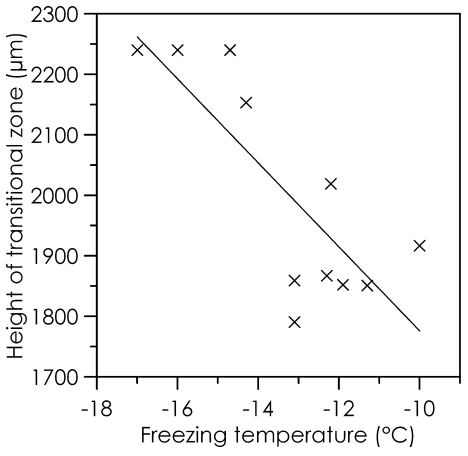

Fig. 7. Height of transitional zone versus freezing temperature. The lower the freezing temperature, the higher the transitional zone.

the supercooling. The closer the freezing temperature from equilibrium temperature, the lower the initial degree of supercooling. The position where the suspension is at equilibrium temperature will be closer to the base of the sample and R-crystals will stop growing earlier, resulting in a shorter transitional zone. With these observations, we show that it is possible to adjust the height of the transitional zone through the control of the initial supercooling, which is dependent on the composition of the suspension, but also on the nucleation conditions, controlled by, among other parameters, the particle size and the shape of the cooling ramp applied. By changing the counter-ion of the dispersant used from NH_4^+ to Na^+, the freezing temperature can be decreased and consequently, the height of the transitional zone can be increased.

IV. Conclusions

The current results allow us to rationalize all previous observations of the transient regime occurring during the solidifi-

cation of colloidal suspension. The cooling conditions, suspensions composition, and characteristics will determine the degree of supercooling reached when the first ice nuclei reach their critical size. The transient regime is determined by this supercooling, and can be controlled to some extent by adjusting the freezing temperature of the suspension or by controlling the nucleation conditions. The later can be achieved by the incorporation of ice nucleation sites, or cooling conditions less favorable to supercooling. These parameters can be used to control the graded structure of the transitional zone, undesirable for applications of porous materials obtained by ice-templating.

Acknowledgments

Financial support was provided by the French National Research Agency (ANR), through the project NACRE BLAN07-2_192446. Beamline access was provided by the ERSF, under the proposal MA997. Acknowledgments are due to local staff of the beamline: Elodie Boller, Paul Tafforeau, and Jean-Paul Valade for the technical and scientific support on the beamline ID-19 at ERSF.

References

[1]T. Fukasawa, M. Ando, T. Ohji, and S. Kanzaki, "Synthesis of Porous Ceramics with Complex Pore Structure by Freeze-dry Processing," *J. Am. Ceram. Soc.*, **84** [1] 230–2 (2001).

[2]S. Deville, "Freeze-Casting of Porous Ceramics: A Review of Current Achievements and Issues," *Adv. Eng. Mater.*, **10** [3] 155–69 (2008).

[3]B.-H. Yoon, W.-Y. Choi, H.-E. Kim, J.-H. Kim, and Y.-H. Koh, "Aligned Porous Alumina Ceramics with High Compressive Strengths for Bone Tissue Engineering," *Scripta Mater.*, **58** [7] 537–40 (2008).

[4]A. Szepes, J. Ulrich, Z. Farkas, J. Kovács, and P. Szabó-Révész, "Freeze-Casting Technique in the Development of Solid Drug Delivery Systems," *Chem. Eng. Process.*, **46** [3] 230–8 (2007).

[5]G. Frank, E. Christian, and D. Koch, "A Novel Production Method for Porous Sound-Absorbing Ceramic Material for High-Temperature Applications," *Int. J. Appl. Ceram. Technol.*, **8** [3] 646–52 (2011).

[6]T. L. Cable, J. A. Setlock, S. C. Farmer, and A. J. Eckel, "Regenerative Performance of the NASA Symmetrical Solid Oxide Fuel Cell Design," *Int. J. Appl. Ceram. Technol.*, **8** [1] 1–12 (2010).

[7]T. L. Cable and S. W. Sofie, "A Symmetrical, Planar SOFC Design for NASA's High Specific Power Density Requirements," *J. Power Sources*, **174** [1] 221–7 (2007).

[8]S.-H. Lee, S.-H. Jun, H.-E. Kim, and Y.-H. Koh, "Fabrication of Porous PZT-PZN Piezoelectric Ceramics with High Hydrostatic Figure of Merits Using Camphene-Based Freeze Casting," *J. Am. Ceram. Soc.*, **90** [9] 2807–13 (2007).

[9]S. Deville, E. Maire, A. Lasalle, A. Bogner, C. Gauthier, J. Leloup, and C. Guizard, "In Situ X-Ray Radiography and Tomography Observations of the Solidification of Aqueous Alumina Particle Suspensions. Part I: Initial Instants," *J. Am. Ceram. Soc.*, **92** [11] 2489–96 (2009).

[10]S. Deville, E. Maire, A. Lasalle, A. Bogner, C. Gauthier, J. Leloup, and C. Guizard, "In Situ X-Ray Radiography and Tomography Observations of the Solidification of Aqueous Alumina Particles Suspensions. Part II: Steady State," *J. Am. Ceram. Soc.*, **92** [11] 2497–503 (2009).

[11]S. Deville, E. Maire, A. Lasalle, A. Bogner, C. Gauthier, J. Leloup, and C. Guizard, "Influence of Particle Size on Ice Nucleation and Growth During the Ice-Templating Process," *J. Am. Ceram. Soc.*, **93** [9] 2507–10 (2010).

[12]A. Bareggi, E. Maire, A. Lasalle, and S. Deville, "Dynamics of the Freezing Front During the Solidification of a Colloidal Alumina Aqueous Suspensions: In Situ X-ray Radiography, Tomography and Modeling," *J. Am. Ceram. Soc.* (2011) early view.

[13]Y. Zhang, L. Hu, and J. Han, "Preparation of a Dense/Porous BiLayered Ceramic by Applying an Electric Field During Freeze Casting," *J. Am. Ceram. Soc.*, **92** [8] 1874–6 (2009).

[14]N. O. Shanti, K. Araki, and J. W. Halloran, "Particle Redistribution During Dendritic Solidification of Particle Suspensions," *J. Am. Ceram. Soc.*, **89** [8] 2444–7 (2006).

[15]J. Buffiere, E. Maire, J. Adrien, J. Masse, and E. Boller, "In Situ Experiments with X ray Tomography: An Attractive Tool for Experimental Mechanics," *Exp. Mech.*, **50** [3] 289–305 (2010).

[16]W. S. Rasband, *ImageJ*, U. S. National Institutes of Health, Bethesda, Maryland, USA, http://imagej.nih.gov/ij/, 1997–2011 and http://pacific.mpi-cbg.de/wiki/index.php/Trainable_Segmentation_Plugin

[17]M. Spannuth, S. G. J. Mochrie, S. S. L. Peppin, and J. S. Wettlaufer, "Particle-Scale Structure in Frozen Colloidal Suspensions from Small-Angle X-ray Scattering," *Phys. Rev. E*, **83** [2] 021402 (2011).

[18]K. Funakoshi, T. Inada, T. Tomita, H. Kawahara, and T. Miyata, "Thermal Hysteresis Induced by Ammonium Polyacrylate as Antifreeze Polymer," *J. Cryst. Growth*, **310** [14] 3342–7 (2008).

[19]J. P. Jolivet, M. Henry, and J. Livage, *(From Solution to Oxide) "De la solution à l'oxyde"*. pp. 387 in EDP Sciences. ed., Paris, 1994. □

Author Query Form

Journal: JACE
Article: 4993

Dear Author,
During the copy-editing of your paper, the following queries arose. Please respond to these by marking up your proofs with the necessary changes/additions. Please write your answers on the query sheet if there is insufficient space on the page proofs. Please write clearly and follow the conventions shown on the attached corrections sheet. If returning the proof by fax do not write too close to the paper's edge. Please remember that illegible mark-ups may delay publication.
Many thanks for your assistance.

Query reference	Query	Remarks
1	**AUTHOR: A running head short title was not supplied; please check if this one is suitable and, if not, please supply a short title of up to 40 characters that can be used instead.**	
2	**AUTHOR: Please check that the title, author names, affiliations, and corresponding author information is listed accurately for publication.**	
3	**AUTHOR: Please check whether "chlorhydric acid" should read as "hydrochloric acid" throughout the text.**	
4	**AUTHOR: Please give address information for 'TA Instruments': town and state.**	
5	**AUTHOR: Please update reference [12].**	
6	**AUTHOR: Figures 3 and 4 have been renumbered to Figures 4 and 3. Similar changes are made in text also. Please check.**	

MARKED PROOF

Please correct and return this set

Please use the proof correction marks shown below for all alterations and corrections. If you wish to return your proof by fax you should ensure that all amendments are written clearly in dark ink and are made well within the page margins.

Instruction to printer	*Textual mark*	*Marginal mark*
Leave unchanged	··· under matter to remain	New matter followed by ⌐ or ⌐(x2)
Insert in text the matter indicated in the margin	⌐	
Delete	/ through single character, rule or underline or ⊢⊣ through all characters to be deleted	⌐/ or ⌐/(x2)
Substitute character or substitute part of one or more word(s)	/ through letter or ⊢⊣ through characters	new character / or new characters /
Change to italics	— under matter to be changed	⌐
Change to capitals	≡ under matter to be changed	≡
Change to small capitals	= under matter to be changed	=
Change to bold type	~ under matter to be changed	~
Change to bold italic	≈ under matter to be changed	≈
Change to lower case	Encircle matter to be changed	≠
Change italic to upright type	(As above)	⌐
Change bold to non-bold type	(As above)	⌐
Insert 'superior' character	/ through character or ⌐ where required	Y or Y under character e.g. Y^{3} or Y^{3}
Insert 'inferior' character	(As above)	⌐ over character e.g. Y_{2}
Insert full stop	(As above)	⊙
Insert comma	(As above)	,
Insert single quotation marks	(As above)	Y or Y and/or Y or Y
Insert double quotation marks	(As above)	Y or Y and/or Y or Y
Insert hyphen	(As above)	⊢
Start new paragraph	⌐	⌐
No new paragraph	⌐	⌐
Transpose	⌐	⌐
Close up	linking ⁀ characters	⁀
Insert or substitute space between characters or words	/ through character or ⌐ where required	Y
Reduce space between characters or words	| between characters or words affected	⊤